HHS Public Access

Author manuscript

J Biomol Struct Dyn. Author manuscript; available in PMC 2024 September 03.

Published in final edited form as:

J Biomol Struct Dyn. 2023 April ; 41(7): 2992–3001. doi:10.1080/07391102.2022.2043938.

Inhibitory mechanism of clioquinol and its derivatives at the exopeptidase site of human angiotensin-converting enzyme-2 and receptor binding domain of SARS-CoV-2 viral spike

Idowu A. Kehinde,
Anu Egbeyemi,
Manvir Kaur,
Collins Onyenaka,
Tolulope Adebusuyi,
Omonike A. Olaleye

Department of Pharmaceutical and Environmental Health Sciences, College of Pharmacy and Health Sciences, Texas Southern University, TX, USA

Abstract

The outbreak of SARS-CoV-2 infections around the world has prompted scientists to explore different approaches to develop therapeutics against COVID-19. This study focused on investigating the mechanism of inhibition of clioquinol (CLQ) and its derivatives (7-bromo-5-chloro-8-hydroxyquinoline (CLBQ), 5, 7-Dichloro-8-hydroxyquinoline (CLCQ)) against the viral glycoprotein, and human angiotensin-converting enzyme-2 (hACE-2) involved in SARS-CoV-2 entry. The drugs were docked at the exopeptidase site of hACE-2 and receptor binding domain (RBD) sites of SARS-CoV-2 S_{gp} to calculate the binding affinity of the drugs. To understand and establish the inhibitory characteristics of the drugs, molecular dynamic (MD) simulation of the best fit docking complex performed. Evaluation of the binding energies of the drugs to hACE-2 after 100 ns MD simulations revealed CLQ to have the highest binding energy value of −40.4 kcal/mol close to MLN-7640 (−45.4 kcal/mol), and higher than the exhibited values for its derivatives: CLBQ (−34.5 kcal/mol) and CLCQ (−24.8 kcal/mol). This suggests that CLQ and CLBQ bind more strongly at the exopeptidase site than CLCQ. Nevertheless, the evaluation of binding affinity of the drugs to SARS-CoV-2 S_{gp} showed the drugs are weakly bound at the RBD site, with CLBQ, CLCQ, CLQ exhibiting relatively low energy values of −16.8 kcal/mol, −16.34 kcal/mol, −12.5 kcal/mol, respectively compared to the reference drug, Bisoxatin (BSX), with a value of −25.8 kcal/mol. The structural analysis further suggests decrease in systems stability and explain the mechanism of inhibition of clioquinol against SARS-CoV-2 as reported in previous *in vitro* study.

CONTACT Idowu A. Kehinde Kehinde.idowu@tsu.edu Department of Pharmaceutical and Environmental Health Sciences, College of Pharmacy and Health Sciences, Texas Southern University, 3100 Cleburne St, Houston, TX77004, USA.

Disclosure statement

No potential conflict of interest was reported by the authors.

Keywords

SARS-CoV-2; clioquinol and its derivatives; exopeptidase; receptor binding domain; molecular dynamic simulation

Introduction

Severe acute respiratory syndrome coronavirus 2 (SARS-CoV-2) is the etiological agent of the coronavirus disease 2019 (COVID-19), which is the current pandemic facing the world. The SARS-CoV-2 virus is a single stranded-RNA virus, belonging to *Coronaviridae* family and order *Nidovirales* (Zhou et al., 2020). The Coronavirinae subfamily of the *Coronaviridae* family is subdivided into four genera (alpha (α), beta (β), gamma (γ), and delta (δ)) (Chan et al., 2020). Coronaviruses are non-segmented and enveloped viruses with diameter ranging between 50 to 200 nm. They have large (about ~30 kb) and single stranded (ss-(+))-RNA genome (Fehr & Perlman, 2015). Aside from SARS-CoV-2, several other coronaviruses have been reported which include HCoV-HKU1, MERS-CoV, HCoVNL63, HCoV-OC43, HCoV-229E (Chan et al., 2020). Unlike most of the coronaviruses known to cause minor symptoms and common cold, SARS-CoV-1, SARS-CoV-2 and MERS-CoV have been associated with causing serious and severe complications to the lower respiratory tracts, spreading to other vital organs. According to Gorbalenya *et al*, SARS-CoV-1 shares approximately 80% genetic similarity with SARS-CoV-2 (Gorbalenya et al., 2020), while bat coronavirus, RaTG13, share a higher genetic similarity of 98% with SARS-CoV-2 (Zhou et al., 2020). Like other coronaviruses, the SARS-CoV-2 is spherically shaped, with Spike (S) glycoproteins that originate from viral surface (Fehr & Perlman, 2015).

Two structural proteins (envelope (E) and membrane (M)) together with the Spike glycoprotein (SARS-CoV-2S_{gp}) comprises the viral envelope, while the nucleocapsid (N) protein binds and protects the RNA genome. The SARS-CoV-2S_{gp} controls essential biological processes such as the attachment to the host cell. The viral attachment occurs via the interaction between the receptor binding domain (RBD) of SARS-CoV-2S_{gp} with the human angiotensin-converting enzyme 2 (hACE-2) receptor (Hoffmann et al., 2020). hACE-2 is a zinc-containing enzyme found on the membrane surface of different cells such as the intestinal enterocytes, kidney cells, and more cells (Donoghue et al., 2000; Hikmet et al., 2020).

Around the world, scientists are using several approaches to target key viral and host cell factors vital for viral replication, therefore, producing many scientific findings enhancing the development of therapeutic agents against COVID-19. Two of the major approaches used are, targeting the intracellular step of viral replication and viral entry into host cells. This study and several others have focused on the inhibition of both the viral and host cells factors involved in SARS-CoV-2 entry. The SARS-CoV-2 S_{gp} is the viral factor used for viral attachment, while hACE-2, transmembrane protease, serine 2 (TMPRSS2) and cathepsin B and L (CatB/L) are host cells factors enhancing viral entry. These factors have become significant target for drug discovery against the disease.

Studies have reported drugs such as zafirlukast, cefopera-zone and phytochemical compounds such as geraniin, Curcumin, cyabnidin-3glucoside, Hesperidin and andrographolide as potential inhibitors of SARS-CoV-2 S_{gp} (Basu et al., 2020; Maurya et al., 2020; Senathilake et al., 2020; Shode et al., 2021). Similarly, many studies have also reported nafamostat, camostat, and 4-(4-guanidinobenzoyloxy) phenylacetic acid (GBPA) to inhibit TMPRSS2 and, being approved to treat SARS-CoV-2 in Japan (Montopoli et al., 2020; Hoffmann et al., 2020a; Yamamoto et al., 2020). Clinical studies have further demonstrated that some of these molecules are effective against SARS-CoV-2. Markus *et al.* reported Bromhexine Hydrochlorides, without severe adverse effects, and clinically effective against COVID-19 (Markus et al., 2020).

Phytochemicals such as Barrigenol, Kaempferol, Myricetin and Theaflavin have been identified as promising inhibitors of nonstructural protein 16 (NSP16) of SARS-CoV-2 (Singh et al., 2021, Sharma et al., 2021). More In silico study have identified more potent and promising inhibitor of SAR-CoV-2 main protease enzyme. Compounds such as DSPD-2, DSPD-6, DSPD-5, Oolonghomobisflavan-A, 6-Hydroxylcyanidin-3-rutinoside, epigallocatechin gallate and kaempferol-7-glucoside were reported to be potent inhibitors of SARS-CoV-2 main protease enzyme (Bhardwaj et al., 2021; Bhardwaj et al., 2021; Shode et al., 2021).

In a previous study from our laboratory, Clioquinol (CLQ) and its derivatives; 7-bromo-5-chloro-8-hydroxyquinoline (CLBQ); and 5, 7-Dichloro-8-hydroxyquinoline (CLCQ) were discovered as potent inhibitors of SARS-CoV-2 infection-induced cytopathic effect. The study reported CLQ, CLBQ and CLCQ as potent inhibitors of SARS-CoV-2, and further reported that the three compounds showed potent anti-exopeptidase activity against recombinant hACE-2 (Olaleye et al., 2021). To further evaluate and establish the molecular mechanisms underlying the CLQ pharmacophore inhibition of SARS-CoV-2 infection, this present study investigated the inhibitory mechanism of Clioquinol and its analogues as potent inhibitors of the viral spike protein and hACE-2 employing a computational approach.

Clioquinol and its derivatives are hydroxyquinoline drugs, used for treatment of fungal drug and protozoal infections. They have been reported to inhibit several enzymes associated with DNA replication, and also reported to inhibit both viral and protozoal infections (Rohde et al., 1976).

Methods

Molecular docking and simulation

Proteins (SARS-CoV-2s_{gp} and hACE2) acquisition and preparation

The X-ray crystal structures of the SARS-CoV-2 S_{gp} (PDB code: 6LZG) and hACE2 (PDB code: 1R4L) were obtained from the RSCB Protein Data Bank (Wang et al., 2020; Towler et al., 2004). The two proteins' structures were then prepared on the UCSF Chimera software package (Yang et al., 2012). The structures of the proteins were prepared by removing water molecules, nonstandard naming, protein residue connectivity. The missing atoms of

sidechains and protein backbone were added to the protein structure before the molecular docking. MLN-4760, a known and experimentally proved inhibitor of hACE-2 was used a reference drug for hACE-2 (Nami et al., 2020; Obakachi et al., 2021), while Bisoxatin (BSX), a laxative drug that has been reported to bind strongly and inhibit SARS-CoV-2 spike protein was used as reference inhibitor for the spike protein (Unni et al., 2020). The 3-D structures of the drugs were prepared on the Avogadro software package (Hanwell et al., 2012).

Molecular docking

Autodock vina available on Chimera version 1.14 was used for molecular docking (Trott & Olson, 2010), with default docking parameters. Before docking, Gasteiger charges were added to the molecules, and the non-polar hydrogen atoms were merged to carbon atoms. The molecules were then docked into the proteins' binding pocket, S1 subunit of the SARS-CoV-2 spike protein (Receptor binding domain (RBD)) and hACE2, by defining the grid box with a spacing of 1 Å each and size and (22 × 41 ×18) and (26 × 24 ×25) pointing in x, y and z directions, respectively. The protonation state of the target was performed before docking calculations. Exhaustiveness number eight was used. The best docking poses for the two drugs were then subjected to molecular dynamics simulations (Figure 1) (Al-Karmalawy et al., 2021).

Molecular dynamic (MD) simulations

The MD simulation was performed as described by Kehinde et al. (2019). The simulations were performed using the GPU version provided with the AMBER package (AMBER 18) (Case et al., 2021), in which the FF18SB variant of the AMBER force field (Nair & Miners, 2014) was used to describe the systems.

ANTECHAMBER was used to generate atomic partial charges for the ligand by utilizing the Restrained Electrostatic Potential (RESP) and the General Amber Force Field (GAFF) procedures. The Leap module of AMBER 18 allowed for the addition of hydrogen atoms and Cl^- and Na + counter ions to COVID-19S_{gp} and hACE2, respectively, to neutralize all systems. The systems were then suspended implicitly within an orthorhombic box of TIP3P water molecules such that all atoms were within 10 Å of any box edge (Jorgensen et al., 1983).

An initial minimization of 2000 steps were carried out with an applied restraint potential of 500 kcal/mol for both solutes. They were performed for 1000 steps using the steepest descent method followed by 1000 steps of conjugate gradients. An additional full minimization of 1000 steps were further carried out using the conjugate gradient algorithm without restraint. A gradual heating MD simulation from 0 K to 300 K was executed for 50 ps, such that the systems maintained a fixed number of atoms and fixed volume. The systems' solutes were imposed with a potential harmonic restraint of 10 kcal/mol and collision frequency of 1.0 ps. Following heating, an equilibration estimating 500 ps of each system was conducted; the operating temperature was kept constant at 300 K. Additional features such as several atoms and pressure were also held constant, mimicking an isobaric-

isothermal ensemble. The system's pressure was maintained at 1 bar using the Berendsen barostat (Gonnet, 2007; Basconi & Shirts, 2013).

The total time for the MD simulations conducted was 100 ns. In each simulation, the SHAKE algorithm was employed to constrict hydrogen atoms' bonds (Ryckaert et al., 1977). The step size of each simulation was 2fs, and an SPFP precision model was used. The simulations coincided with the isobaric-isothermal ensemble (NPT), with randomized seeding, the constant pressure of 1 bar maintained by the Berendsen barostat (Basconi & Shirts, 2013), a pressure-coupling constant of 2 ps, a temperature of 300 K and Langevin thermostat (Izaguirre et al., 2001) with a collision frequency of 1.0 ps.

Post-dynamic analysis and binding free energy calculations

Analysis of root mean square deviation (RMSD), root means square fluctuation (RMSF), and radius of gyration (RoG) was done using the CPPTRAJ module employed in the AMBER 18 suit. All raw data plots were generated using the Origin data analysis software (Seifert, 2014).

To estimate and compare the systems' binding affinity, the free binding energy was calculated using the Molecular Mechanics/GB Surface Area method (MM/GBSA) (Ylilauri & Pentikäinen, 2013). Binding free energy was averaged over 100000 snapshots extracted from the 100 ns trajectory. The free binding energy (ΔG) computed by this method for each molecular species (complex, ligand, and receptor) can be represented as:

$$\Delta G_{bind} = G_{complex} - G_{receptor} - G_{ligand} \quad (1)$$

$$\Delta G_{bind} = E_{gas} + G_{sol} - TS \quad (2)$$

$$E_{gas} = E_{int} + E_{vdw} + E_{ele} \quad (3)$$

$$G_{sol} = G_{GB} + G_{SA} \quad (4)$$

$$G_{SA} = \gamma SASA \quad (5)$$

E_{gas} denotes the gas-phase energy, which consists of the internal energy E_{int}, Coulomb energy E_{ele} and the van der Waals energies E_{vdw}. The E_{gas} was directly estimated from the FF14SB

force field terms. Solvation free energy, G_{sol}, was estimated from the energy contribution from the polar states, GGB, and non-polar states, G. The non-polar solvation energy, SA. GSA was determined from the solvent-accessible surface area (SASA), using a water probe radius of 1.4 Å. In contrast, the polar solvation, GGB, the contribution was estimated by solving the GB equation. S and T denote the total entropy of the solute and temperature, respectively.

Results and discussion

Thermodynamic binding free energy of clioquinol and its analogues to hACE-2 and spike protein

Our laboratory, in efforts to proffer therapeutic solutions for COVID-19, conducted the first *in vitro* study to repurpose Clioquinol and its analogues as potent inhibitors of SARS-CoV-2 infection, and reported CLQ, CLBQ and CLCQ as potent inhibitors of SARS-CoV-2 infection (Olaleye et al., 2021). To further evaluate and establish the molecular mechanisms underlying of Clioquinol inhibition of SARS-CoV-2 infection, this study investigated the inhibitory mechanism of Clioquinol and its analogues as potent inhibitors of the viral spike protein and hACE-2. The drugs were docked at the exopeptidase site of hACE-2 and the RBD site of SARS-CoV2 S_{gp} to calculate the binding affinity of the drugs to the two proteins (Table 1). Figure 2 showed the plot of binding energy versus the time over the simulation time to establish the stability of the bindings.

Molecular Docking measures the fitness of each drug at the binding sites of each protein. An evaluation of the binding energies of the drugs and the reference drug, MLN-4760 at the exopeptidase site of hACE-2 revealed that MLN showed the highest binding energy of −45.4 kcal/mol, while CLQ showed a relatively close binding energy value of −40.4 kcal/mol. CLBQ and CLCQ exhibited binding energy values of −34.4 kcal/mol and −24.8 kcal/mol). This finding suggests CLQ, and CLBQ bind better at the exopeptidase site than CLCQ when compared with the reference drug, and they might be inhibitors. This *in silico* study's result, therefore, correlate with the *in vitro* study that reported anti-exopeptidase activity of the three drugs against hACE-2, with CLQ being the most potent amongst all three analogues tested at IC_{50} of 5.36 μM, follow by CLBQ (5.55 μM, IC_{50}) and CLCQ (<10 μM, IC_{50}) (Olaleye et al., 2021). In a separate study by Obakachi *et al.* to identify potent inhibitors of hACE-2, potent and promising inhibitors of hACE-2 (7 h, 7 b, 7k and 8d) with relatively low binding energy than the reference drugs were identified (Obakachi et al., 2021). It is however uncommon to find promising compounds with relatively lower binding energy than the reference drug(s).

However, the evaluation of binding affinity of the drugs to SARS-CoV-2 S_{gp} showed the drugs are weakly bind at the RBD site, with CLBQ, CLCQ, CLQ exhibiting binding energy values of −16.8 kcal/mol, −16.3 kcal/mol, and −12.4 kcal/mol, respectively (Table 2), when compared with the reference drug (BSX) with binding energy values of −25.8 kcal/mol. This suggests the drugs possess week affinity to the spike protein, which corroborate the result of the previous in vitro study by Olaleye *et al.* (Olaleye et al., 2021).

Subsequent, from these findings, it might be inferred that the drugs possess strong affinity to hACE-2, which might be the basis step of their inhibitory activities against hACE-2 as seen from the *in vitro* study by Olaleye *et al.* (Olaleye et al., 2021).

To further understand and establish the mechanistic inhibitory characteristics of the drugs through their interaction with the amino residues at the exopeptidase site of hACE-2 and RBD site of SARS-CoV-2 S_{gp}, 2 D plots of ligand-protein interactions were plotted for each drug and reference drug. Several studies have examined and reported ligand-protein interaction plots at the exopeptidase site of hACE-2 and RBD sites of SARS-CoV-2 S_{gp} (Unni et al., 2020; Nami et al., 2020; Shode et al., 2021; Obakachi et al., 2021). As shown in Figures 2 and 4, the plots showed different types of interactions (Van der Waals (vdW) overlaps, hydrogen bond (Hbond), alkyl, π-alkyl, π - π stacked interaction, and π - π T-shaped interactions) that exist between the drugs and the two proteins. From the hACE-2 protein-ligand interaction analysis (Figure 3a), the plot revealed that MLN-4760 binds strongly with hACE-2 with more interaction bonds than the other drugs, which might be responsible for its higher binding energy. A total of 20 interaction bonds with total 11 conventional Hbond and carbon hydrogen bonds, 5pi-alkyl and pi-cation bonds each. CLQ on the other hand, strongly bonded to hACE2 through 12 hydrogen bonds with residues Thr427, Gln424, Leu392, Ser391, Glu388, His356, Arg500, Arg255, Tyr497, Tyr353, Asp349 and Thr258, 2pi-Alkyl bonds with

Phe256 and Ala395 and 1 pi-pi T-shaped bond. CLBQ binds to hACE-2 with a total of 10 bonds: 5 hydrogen bonds with residues Thr258, bonds with residues Thr258, Thr427, Thr353 and Arg255, 3 strong pi-pi T-shaped bonds with His356, Leu353 and Phe256, and 2 pi-Alkyl bonds with Pro328 and Tyr497. Nine (9) bonds; 6 Hbond, 1 pi-pi stacked and 2 pi-Alkyl bonds were observed with CLCQ binding at the exopeptidase site of hACE-2. The high numbers of total interactions and Hbonds observed in MLN-4760 and CLQ bindings correlate with their high binding free binding energy values recorded in Table 1. An evaluation of the bond length of all the main hydrogen bonds showed CLQ had three close hydrogen bond interactions with active site residues (Ser391, (3.98 Å), Glu388, (4.11 Å) and Thr353, (6.15 Å)), while MLN and CLCQ had one closed hydrogen of with the residues at Tyr497 (5.57 Å) and Pro328 (3.96 Å), respectively. These hydrogen interactions might suggest the possibility of the compounds inhibiting ACE-2, as hydrogen interaction is essential forACE-2 inhibition (Al-Karmalawy et al., 2021). Another similar *in silico* study by Nami *et al.* reported a high number of Hbonds (10) was observed after the binding of MLN-4670 of hACE-2 at the exopeptidase site (Nami et al., 2020). Although 5 Hbonds was observed in CLBQ, but the presence of 3 strong pi-pi stacked interactions makes it to exhibited higher binding energy than CLCQ with higher Hbond and total interactions.

Figure 4 showed the protein-ligand interactions analysis plot of the drugs with SARS-CoV-2 $S_{gp.}$ The reference drug, BSX binds more strongly with a total of 9 conventional Hbonds and carbon hydrogen bonds with Ag71, Tyr163, Asn169, Gly164, Gln166, Gly115, Tyr117, Phe165, and Tyr173. CLBQ binds with the spike protein with 6 Hbonds at residues Gln493, Lys417, Gln409, Glu406, Val350 and Ser494, 3 Alkyl bonds, and 1 pi-pi stacked and pi-cation each. CLQ and CLCQ bind with SARS-CoV-2 S_{gp} with a total of 9 bonds each: 4 and 6 Hbonds, respectively. No close contact hydrogen bond interaction was recorded

in all the tested drugs, however, three hydrogen bond interactions with residues Tyr505 (5.03 Å), Gln498 (4.87 Å) and Asn501 (4.86 Å) were observed in the reference drug, BSX. This finding further confirm that the tested drug are not inhibitors of the spike protein as hydrogen bond interactions between spike protein and potential inhibitor is essential for inhibition (Xu et al., 2020; Teli et al., 2020).

Dynamic stability and flexibility of hACE-2 and SARS-CoV-2s_{gp} bound and unbound complexes

To confirm the dynamic of the systems, 100 ns MD simulations was performed. From the RMSD plot (Figure 5), after maintaining convergence at approximately 15 ns all the complexes exhibited favorable stability throughout the MD simulations. For the hACE-2 complexes, the average RMSD of the complexes (Table 3) showed that MLN-4760 and CLBQ complexes have the lowest RMSD values of 1.62 Å and 1.57 Å, respectively when compared with the unbound hACE-2 system, with average value of 1.81. The bindings of CLQ and CLCQ slightly raised the average RMSD values to 1.91 Å and 1.85 Å, respectively. The plot Of the RMSD revealed that both the bound and unbound complexes exhibited stable conformation as evidenced by the relatively low RMSD values recorded. A similar observation was earlier reported in a separate study by Obakachi *et al.* that binding of ligands raised the RMSD values for hACE-2, and stable protein structure was maintained, as demonstrated by lower RMSD plots (Obakachi et al., 2021). Figure 6 showed the RMSD plots for the SARS-CoV-2 S_{gp} complexes. As shown in table 4, the unbound SARS-CoV-2 S_{gp} and CLQ complexes exhibited the lowest RMSD average values of 2.06 Å and 2.09 Å, respectively. However, the binding of the BSX (reference drug), CLBQ and CLCQ raised the average RMSD values to 2.25 Å, 2.86 Å and 2.37 Å, respectively, when compared to the RMSD value of the unbound SARS-CoV2 S_{gp} (2.06 Å). The plots further showed conformational change occurred at the binding of CLBQ, BSX and CLCQ complexes. This observed conformational change of CLQ might be due to orientational modification to accurately fit into the spike RBD site. However, the relatively low RMSD values exhibited by the complexes revealed the structural stability of the protein (SARS-CoV-2 S_{gp}) was not altered, even though the binding affinity and interaction plot's results do not suggest they might be potent inhibitor of SARS-CoV-2 S_{gp}.

To understand the compactness of the alpha carbon backbones of the protein, RoG values for the complexes were investigated. RoG measures the degree of compactness of the alpha carbon backbones of the protein. Figures 4 and 5 showed the RoG plots for all the systems, and table 3, showed the average RoG values for the hACE-2 systems. The result revealed the unbound hACE-2 the highest average RoG values of 24.03 Å, with the drugs, MLN-4760, CLQ, CLBQ and CLCQ exhibiting average RoG values of 23.79 Å, 23.69 Å, 23.91 Å and 23.90 Å, respectively. Low RoG values exhibited by the drugs indicates an increase structural compactness suggesting less mobility. This further validate the structural stability recorded under the RMSD plot. As shown in Figure 6, for the spike protein, the unbound protein exhibited the lowest RoG value of 18.32 Å. However, the binding of the BSX, CLQ and CLCQ insignificantly raised the average RoG values, but the binding of CLBQ raised the average RMSD compared to the unbound complex (Table 3). This increased

average RoG values implies a decrease in protein structure compactness, thereby suggesting increased flexibility (Emmanuel et al., 2019).

To quantifies the enzymes exposure to solvent molecules, the SASA plots for all the systems were investigated. High SASA values is an indication of decrease in the exposure of buried hydrophobic residues which suggest decrease in systems stability (Emmanuel et al., 2019; Ogidigo et al., 2020). The result of average SASA values for the hACE-2 system (Table 3) derived from Figure 5, showed that all the drugs (including the reference drug) slightly lower average SASA values compared to the unbound hACE-2 system. Therefore, this observed, slightly lowered SAS values amongst the drugs complexes is an indication of an increase in the exposure of buried hydrophobic residues which suggest increase in the complexes' stability. This finding might explain the molecular dynamic mechanism of inhibition of clioquinol and its derivatives against SARS-CoV-2. Unlike the hACE-2 complexes, the average SASA values for BSX, CLQ, and CLBQ drugs are higher than the unbound SARS-CoV-2 S_{gp} and CLCQ complexes, suggesting an increase in the stability BSX, CLBQ and CLQ complexes than the unbound protein and CLCQ complexes.

Figures 5 to 6 and Tables 3 to 4 showed the RMSF plots and the average RMSF values for the hACE-2 and SARS-CoV-2 S_{gp} complexes, respectively. This is a measure of the impacts of binding of molecules on the behavior of the active residue (Kumar et al., 2014). High RMSF values indicated increase flexibility movements, and in contrast, lower values conveyed restricted fluctuations. From Table 3, the unbound hACE-2 and CLCQ complexes showed the lowest average RMSF values of 1.14 Å and 1.37 Å, respectively. On the other hand, the binding of MLN-4760, CLQ and CLBQ lowers the RMSF compared to the unbound hACE-2 complexes. This finding together with the SASA, RMSD and RoG results further explains that clioquinol and its derivatives alters the structural conformation of hACE-2 to exert their inhibitory potentials.

For the SARS-CoV-2 S_{gp} systems, higher residues movement was observed as evidenced by high average RMSF values recorded. The unbound protein and CLBQ complex had the highest RMSF values of 12.49 Å and 12.93 Å, respectively. The binding of the reference drug, BSX, CLQ, and CLBQ lowers the RMSF values to 8.19 Å, 10.22 Å, 11.46Å, respectively. This high flexibility movement observed for the drugs might be another indication of orientational modification to accurately fit into the spike RBD site, as also observed in the RMSD plots.

Conclusion

SARS-CoV-2S_{gp} is an essential protein vital for the viral attachment to the host cell through the molecular interaction of the SARS-CoV-2S_{gp} RBD and hACE-2. Therefore, inhibition of these two proteins is a significant step in controlling the viral infectivity. Previous studies from our lab reported CLQ, CLBQ and CLCQ possess anti-exopeptidase activity against hACE-2 and were found to be potent inhibitors of SARS-CoV-2 infection-induced cytopathic effect. In this study, we evaluated and established the molecular mechanism of inhibition of these drugs against hACE-2 and SARS-CoV-2S_{gp} utilizing computational techniques. This study showed Clioquinol and it two derivatives exhibited

anti-exopeptidase activity against hACE-2 by strongly binding to the enzyme and altering the enzyme's structural conformation, which possibly lowered the enzyme's interaction with SARS-CoV2S_{gp}. The study further revealed that Clioquinol and its derivatives weakly bind to SARS-CoV-2S_{gp} at the RBD site, and conformational analysis suggests that the compounds cause high flexibility of SARS-CoV-2S_{gp} amino structure leading to orientational modification to accurately fit into the spike RBD site. This study provides further information on the possibility of repurposing clioquinol and its derivative as alternative treatment for COVID-19 as promising inhibitors of hACE-2.

Funding

This study is funded by NIH grant no U54MD007605.

References

Al-Karmalawy AA, Dahab MA, Metwaly AM, Elhady SS, Elkaeed EB, Eissa IH, & Darwish KM (2021). Molecular docking and dynamics simulation revealed the potential inhibitory activity of ACEIs against SARS-CoV-2 targeting the hACE2 receptor. Frontiers in Chemistry, 9, 661230. 10.3389/fchem.2021.661230

Basconi JE, & Shirts MR (2013). Effects of temperature control algorithms on transport properties and kinetics in molecular dynamics simulations. Journal of Chemical Theory and Computation, 9(7), 2887–2899. 10.1021/ct400109a [PubMed: 26583973]

Basu A, Sarkar A, & Maulik U. (2020). Computational approach for the design of potential spike protein binding natural compounds in SARS-CoV2.Pharmacodynamics, 4, 1–22. 10.21203/rs.3.rs-33181/v1.

Bhardwaj VK, Singh R, Sharma J, Rajendran V, Purohit R, & Kumar S. (2021). Identification of bioactive molecules from tea plant as SARS-CoV-2 main protease inhibitors. Journal of Biomolecular Structure & Dynamics, 39(10), 3449–3458. 10.1080/07391102.2020.1766572 [PubMed: 32397940]

Bhardwaj VK, Singh R, Das P, & Purohit R. (2021). Evaluation of acridinedione analogs as potential SARS-CoV-2 main protease inhibitors and their comparison with repurposed anti-viral drugs. Computers in Biology and Medicine, 128, 104117. 10.1016/j.compbiomed.2020.104117

Case DA, Aktulga HM,K, Belfon IY, Ben-Shalom SR, Brozell DS, Cerutti TE, Cheatham GA Iii, Cisneros VWD, Cruzeiro TA, Darden RE, Duke G, Giambasu MK, Gilson H, Gohlke AW, Goetz R, Harris S, Izadi SA, Izmailov C, Jin K, Kasavajhala MC, Kaymak E, King A, Kovalenko T, Kurtzman TS, Lee S, LeGrand P, Li C, Lin J, Liu T, Luchko R, Luo M, Machado V, Man M, Manathunga KM, Merz Y, Miao O, Mikhailovskii G, Monard H, Nguyen KA, O'Hearn A, Onufriev F, Pan, Pantano R, Qi A, Rahnamoun DR, Roe A, Roitberg C, Sagui S, Schott-Verdugo J, Shen CL, Simmerling NR, Skrynnikov J, Smith J, Swails RC, Walker J, Wang H, Wei RM, Wolf X, Wu Y, Xue DM, York, Zhao PA & Kollman, (2021). Amber 2021. University of California.

Chan JFW, Kok KH, Zhu Z, Chu H, To KKW, Yuan S, & Yuen KY (2020). Genomic characterization of the 2019 novel human-pathogenic coronavirus isolated from a patient with atypical pneumonia after visiting Wuhan. Emerging Microbes & Infections, 9(1), 221–236. 10.1080/22221751.2020.1719902 [PubMed: 31987001]

Donoghue M, Hsieh F, Baronas E, Godbout K, Gosselin M, Stagliano N, Donovan M, Woolf B, Robison K, Jeyaseelan R, Breitbart RE, & Acton S. (2000). A novel angiotensin-converting enzyme-related carboxypeptidase (ACE2) converts angiotensin I to angiotensin 1–9. Circulation Research, 87 (5), e1–e9. 10.1161/01.RES.87.5.e1. [PubMed: 10969042]

Emmanuel IA, Olotu F, Agoni C, & Soliman ME (2019). Broadening the horizon: Integrative pharmacophore-based and cheminformatics screening of novel chemical modulators of mitochondria ATP synthase towards interventive Alzheimer's disease therapy. Medical Hypotheses, 130, 109277. 10.1016/j.mehy.2019.109277

Fehr AR, & Perlman S. (2015). Coronaviruses: An overview of their replication and pathogenesis. In Coronaviruses: Methods and Protocols (Vol. 1282, pp. 1–23). Springer. 10.1007/978-1-4939-2438-7_1.

Gonnet P. (2007). P-SHAKE: A quadratically convergent SHAKE in O(n2). Journal of Computational Physics, 220(2), 740–750. 10.1016/j.jcp.2006.05.032

Gorbalenya AE, Baker SC, Baric RS, de Groot RJ, Drosten C, Gulyaeva AA, Haagmans BL, Lauber C, Leontovich AM, & Neuman BW (2020). The species severe acute respiratory syndrome-related coronavirus: Classifying 2019-nCoV and naming it SARS-CoV-2. Nature Microbiology, 5, 536–544.

Hanwell MD, Curtis DE, Lonie DC, Vandermeerschd T, Zurek E, & Hutchison GR (2012). Avogadro: An advanced semantic chemical editor, visualization, and analysis platform. Journal of Cheminformatics, 4(8), 1–17. [PubMed: 22236646]

Hikmet F, Méar L, Edvinsson Å, Micke P, Uhlén M, & Lindskog C. (2020). The protein expression profile of ACE2 in human tissues. Molecular Systems Biology, 16(7), 1–16. 10.15252/msb.20209610

Hoffmann M, Kleine-Weber H, Schroeder S, Krüger N, Herrler T, Erichsen S, Schiergens TS, Herrler G, Wu N-H, Nitsche A, Müller MA, Drosten C, & Pöhlmann S. (2020). SARS-CoV-2 cell entry depends on ACE2 and TMPRSS2 and is blocked by a clinically proven protease inhibitor. Cell, 181(2), 271–280. 10.1016/j.cell.2020.02.052 [PubMed: 32142651]

Hoffmann M, Schroeder S, Kleine-Weber H, Müller MA, Drosten C, & Pöhlmann S. (2020a). Nafamostat mesylate blocks activation of SARS-CoV-2: New treatment option for COVID-19. Antimicrobial Agents and Chemotherapy, 64(6), e00754–20. 10.1128/AAC.00754-20.

Izaguirre JA, Catarello DP, Wozniak JM, & Skeel RD (2001). Langevin stabilization of molecular dynamics. The Journal of Chemical Physics, 114(5), 2090–2098. 10.1063/1.1332996

Jorgensen WL, Chandrasekhar J, Madura JD, Impey RW, & Klein ML (1983). Comparison of simple potential functions for simulating liquid water. The Journal of Chemical Physics, 79(2), 926–935. 10.1063/1.445869

Kehinde I, Ramharack P, Nlooto M, & Gordon M. (2019). The pharmacokinetic properties of HIV-1 protease inhibitors: A computational perspective on herbal phytochemicals. Heliyon, 5(10), e02565. 10.1016/j.heliyon.2019.e02565

Kumar CV, Swetha RG, Anbarasu A, & Ramaiah S. (2014). Computational analysis reveals the association of threonine 118 methionine mutation in PMP22 resulting in CMT-1A. Advances in Bioinformatics, 2014, 1–10. 10.1155/2014/502618

Markus D, Gottfried L,MM, Marina, Dario B,D, & de V. (2020). "A SARS-CoV-2 Prophylactic and Treatment; A Counter Argument against the Sole Use of Chloroquine, 8(4),1–4. AJBSR.MS.ID.001283. 10.34297/AJBSR.2020.08.001283.

Maurya VK, Kumar S, Bhatt MLB, & Saxena SK (2020). Therapeutic development and drugs for the treatment of COVID-19. Nature Public Health Emergency Collection, 1, 109–126. 10.1007/978-981-15-4814-7_10.

Montopoli M, Zumerle S, Vettor R, Rugge M, Zorzi M, Catapano CV, Carbone GM, Cavalli A, Pagano F, Ragazzi E, Prayer-Galetti T, & Alimonti A. (2020). Androgen-deprivation therapies for prostate cancer and risk of infection by SARS-CoV-2: A population-based study (N= 4532). Annals of Oncology, 31(8), 1040–1045. 10.1016/j.annonc.2020.04.479 [PubMed: 32387456]

Nair PC, & Miners JO (2014). Molecular dynamics simulations: From structure function relationships to drug discovery. Silico Pharm, 2(1), 1–4. 10.1186/s40203-014-0004-8.

Nami B, Ghanaiyan A, Ghanaeian K, & Nami N, (2020). The effect of ACE2 inhibitor MLN-4760 on the interaction of SARS-CoV-2 spike protein with human ACE2: A molecular dynamics study. ChemRxiv, 1, 4–16. 10.26434/chemrxiv.12159945.

Obakachi VA, Kushwaha ND, Kushwaha B, Mahlalela MC, Shinde SR, Kehinde I, & Karpoormath R. (2021). Design and synthesis of pyrazolone-based compounds as potent blockers of SARS-CoV-2 viral entry into the host cells. Journal of Molecular Structure, 1241, 130665. 10.1016/j.molstruc.2021.130665

Ogidigo JO, Iwuchukwu EA, Ibeji CU, Okpalefe O, & Soliman MES (2020). Natural phyto, compounds as possible noncovalent inhibitors against SARS-CoV2 protease:

Computational approach. Journal of Biomolecular Structure and Dynamics, 2, 1–18. 10.1080/07391102.2020.1837681

Olaleye OA, Kaur M, Onyenaka C, & Adebusuyi T. (2021). Discovery of Clioquinol and analogues as novel inhibitors of severe acute respiratory syndrome coronavirus 2 infection, ACE2 and ACE2 – Spike protein interaction in vitro. Heliyon, 7(3), e06426. 10.1016/j.heliyon.2021.e06426

Rohde W, Mikelens P, Jackson J, Blackman J, Whitcher J, & Levinson W. (1976). Hydroxyquinolines inhibit ribonucleic acid-dependent deoxyribonucleic acid polymerase and inactivate Rous sarcoma virus and herpes simplex virus. Antimicrobial Agents and Chemotherapy, 10 (2), 234–240. 10.1128/aac.10.2.234 [PubMed: 185949]

Ryckaert JP, Ciccotti G, & Berendsen HJ (1977). Numerical integration of the Cartesian equations of motion of a system with constraints: Molecular dynamics of n-alkanes. Journal of Computational Physics, 23(3), 327–341. 10.1016/0021-9991(77)90098-5

Seifert E. (2014). OriginPro 9.1: Scientific data analysis and graphing software-software review. Journal of Chemical Information and Modeling, 54(5), 1552–1552. 10.1021/ci500161d [PubMed: 24702057]

Senathilake K, Samarakoon S, & Tennekoon K. (2020). Virtual screening of inhibitors against spike glycoprotein of 2019 novel corona virus: A drug repurposing approach. 10.20944/preprints202003.0042.v1.

Sharma J, Kumar Bhardwaj V, Singh R, Rajendran V, Purohit R, & Kumar S. (2021). An in-silico evaluation of different bioactive molecules of tea for their inhibition potency against non structural protein-15 of SARS-CoV-2. Food Chemistry, 346, 128933. 10.1016/j.foodchem.2020.128933.

Shode FO, Idowu A, Uhomoibhi OJ, & Sabiu S. (2021). Repurposing drugs and identification of inhibitors of integral proteins (spike protein and main protease) of SARS-CoV-2. Journal of Biomolecular Structure and Dynamics, 1, 1–16. Advance online publication. 10.1080/07391102.2021.1886993

Singh R, Bhardwaj VK, Sharma J, Purohit R, & Kumar S. (2021). In-silico evaluation of bioactive compounds from tea as potential SARS-CoV-2 nonstructural protein 16 inhibitors. Journal of Traditional and Complementary Medicine, 2. 10.1016/j.jtcme.2021.05.005.

Teli DM, Shah MB, & Chhabria MT (2020). In silico screening of natural compounds as potential inhibitors of SARS-CoV-2 main protease and spike RBD: Targets for COVID-19. Frontiers in Molecular Biosciences, 7, 599079. 10.3389/fmolb.2020.599079

Towler P, Staker B, Prasad SG, Menon S, Tang J, Parsons T, Ryan D, Fisher M, Williams D, Dales NA, Patane MA, & Pantoliano MW (2004). ACE2 X-ray structures reveal a large hinge-bending motion important for inhibitor binding and catalysis. Journal of Biological Chemistry, 279(17), 17996–18007. 10.1074/jbc.M311191200 [PubMed: 14754895]

Trott O, & Olson AJ (2010). AutoDock Vina: Improving the speed and accuracy of docking with a new scoring function, efficient optimization, and multithreading. Journal of Computational Chemistry, 31, 455–461. [PubMed: 19499576]

Unn S., Aout S., Thiyagarajan S., & Padmanabha B. (2020). Identification of a repurposed drug as an inhibitor of Spike protein of human coronavirus SARS-CoV-2 by computational methods. Journal of Biosciences, 45(1), 130. 10.1007/s12038-020-00102-w [PubMed: 33184246]

Wang Q, Zhang Y, Wu L, Niu S, Song C, Zhang Z, Lu G, Qiao C, Hu Y, Yuen KY, Wang Q, Zhou H, Yan J, & Qi J. (2020). Structural and functional basis of SARS-CoV-2 entry by using human ACE2. Cell, 181(4), 894–904.e9. 10.1016/j.cell.2020.03.045 [PubMed: 32275855]

Xu J, Zhao S, Teng T, Abdalla AE, Zhu W, Xie L, Wang Y, & Guo X. (2020). Systematic comparison of two animal-to-human transmitted human coronaviruses: SARS-CoV-2 and SARS-CoV. Viruses, 12(2), 244. 10.3390/v12020244 [PubMed: 32098422]

Yamamoto M, Kiso M, Sakai-Tagawa Y, Iwatsuki-Horimoto K, Imai M, Takeda M, Kinoshita N, Ohmagari N, Gohda J, Semba K, Matsuda Z, Kawaguchi Y, Kawaoka Y, & Inoue JI (2020). The anticoagulant nafamostat potently inhibits SARS-CoV-2S protein-mediated fusion in a cell fusion assay system and viral infection in vitro in a cell-type-dependent manner. Viruses, 12(6), 629. 10.3390/v12060629 [PubMed: 32532094]

Yang Z, Lasker K, Schneidman-Duhovny D, Webb B, Huang CC, Pettersen EF, Goddard TD, Meng EC, Sali A, & Ferrin TE (2012). UCSF chimera, MODELLER, and IMP: An integrated modeling

system. Journal of Structural Biology, 179(3), 269–278. 10.1016/j.jsb.2011.09.006 [PubMed: 21963794]

Ylilauri M, & Pentikäinen OT (2013). MMGBSA as a tool to understand the binding affinities of filamin-peptide interactions. Journal of Chemical Information and Modeling, 53(10), 2626–2633. 10.1021/ci4002475 [PubMed: 23988151]

Zhou P, Yang X-L, Wang X-G, Hu B, Zhang L, Zhang W, Si H-R, Zhu Y, Li B, Huang C-L, Chen H-D, Chen J, Luo Y, Guo H, Jiang R-D, Liu M-Q, Chen Y, Shen X-R, Wang X, … Shi Z-L (2020). A pneumonia outbreak associated with a new coronavirus of probable bat origin. Nature, 588(7836), 270–273. 10.1038/s41586-020-2951-z

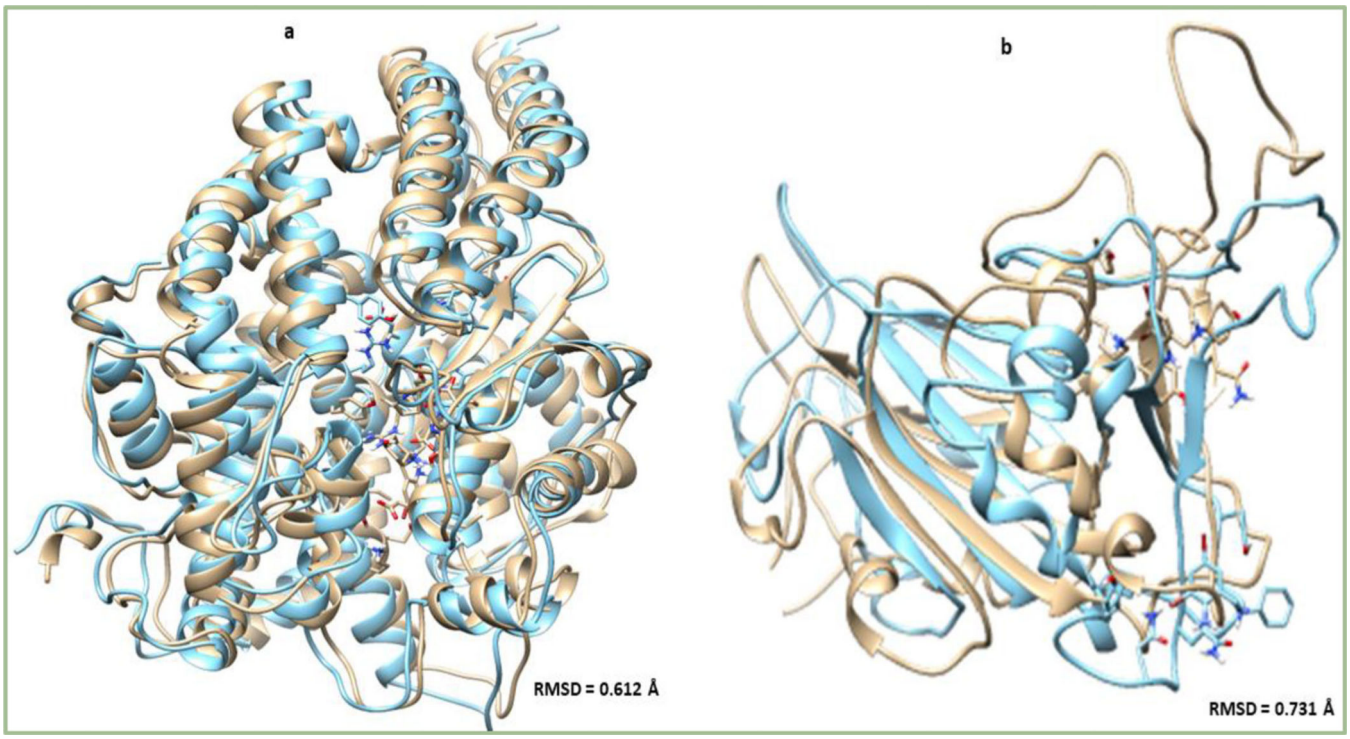

Figure 1.

Superimpositions of the crystalized structures of ligand-complexes of a). hCAE2 and b). SARS-CoV-2 Spike gps with their respective RMSD values.

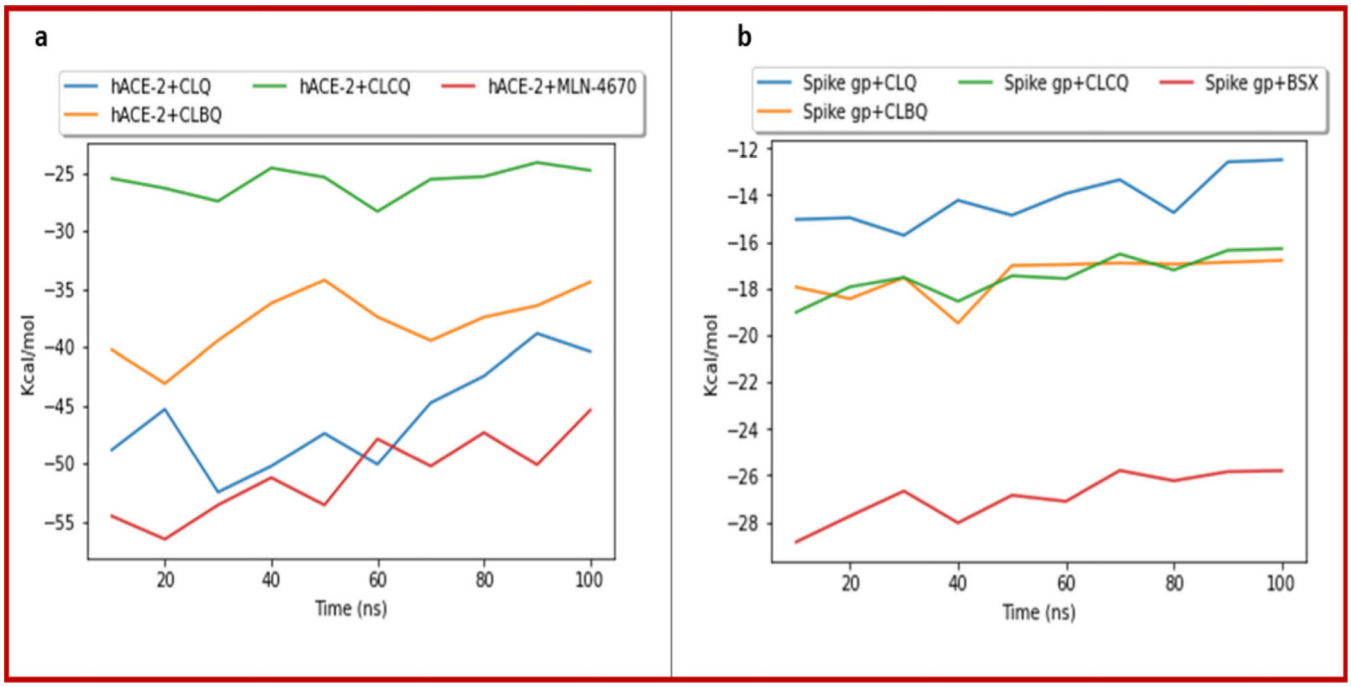

Figure 2.

A plot of binding energies vs. time over the 100 ns MD simulations Protein-ligand interaction of Clioquinol and its analogues to hACE-2 and SARS-CoV-2 S_{gp}.

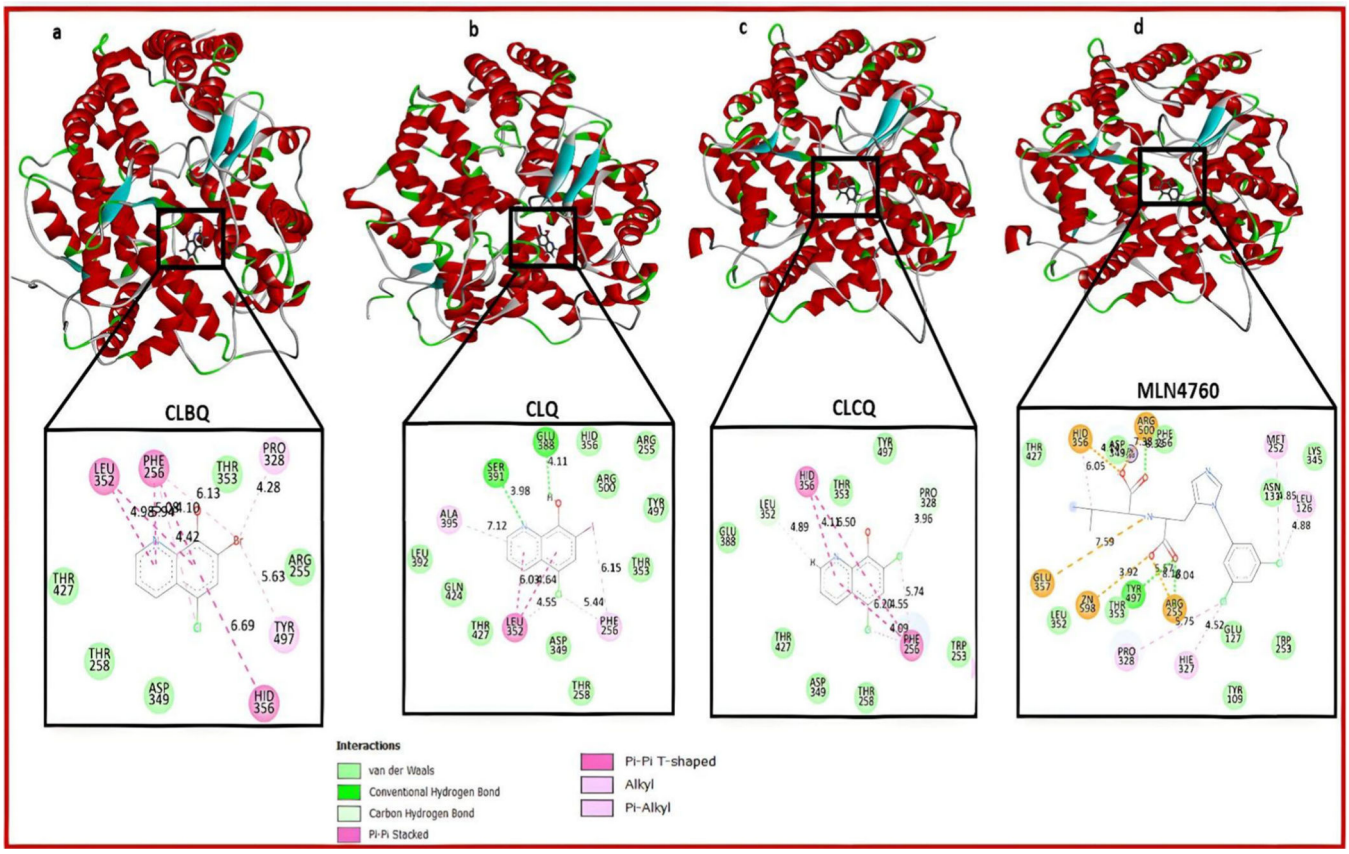

Figure 3.

Representation of Protein (hACE-2)-ligand interactions plots with different amino acid residues of a) CLBQ, b) CLQ and c) CLCQ.

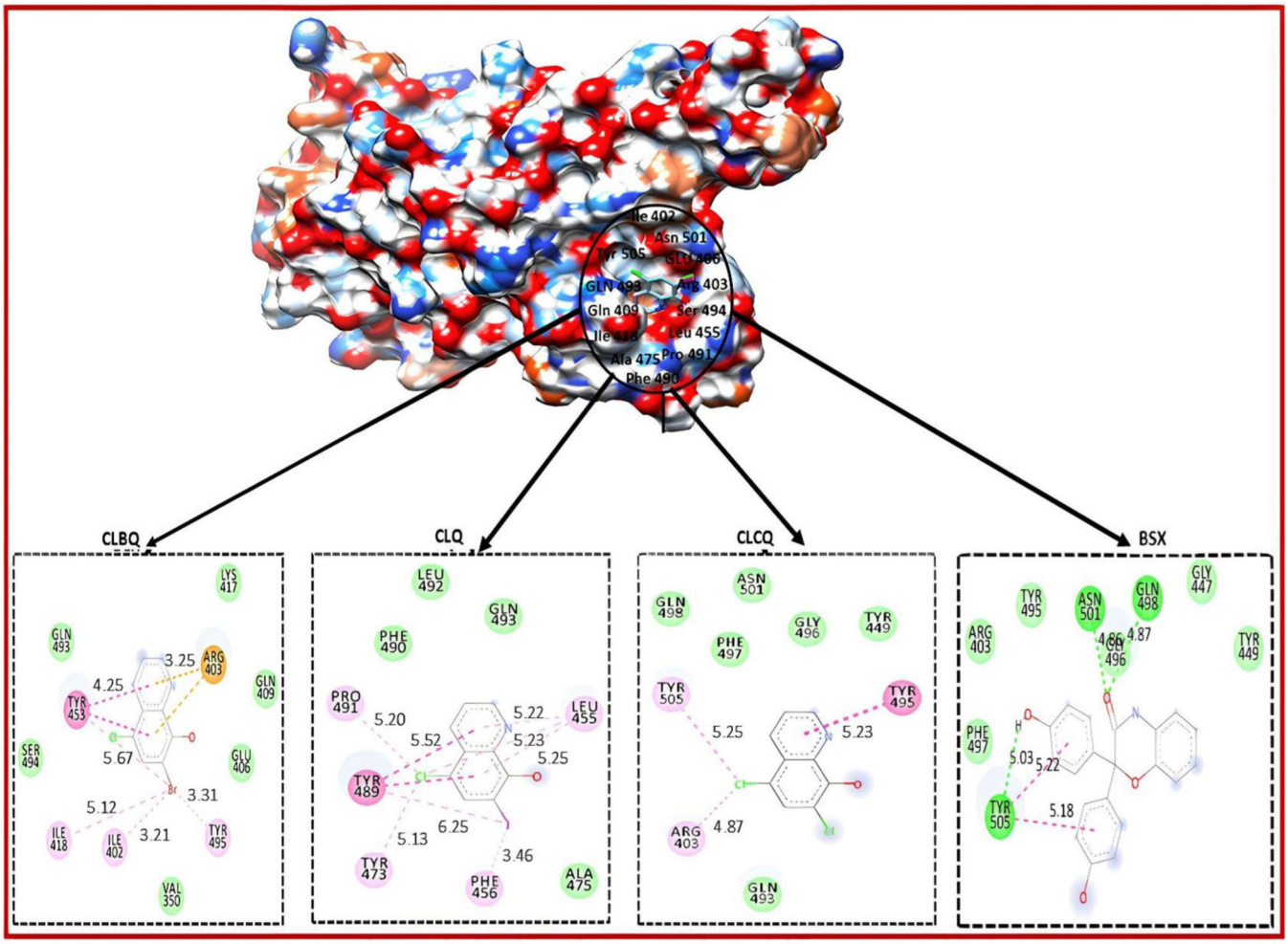

Figure 4.

Representation of Protein (Spike gp)-ligand interactions plot with different amino acid residues.

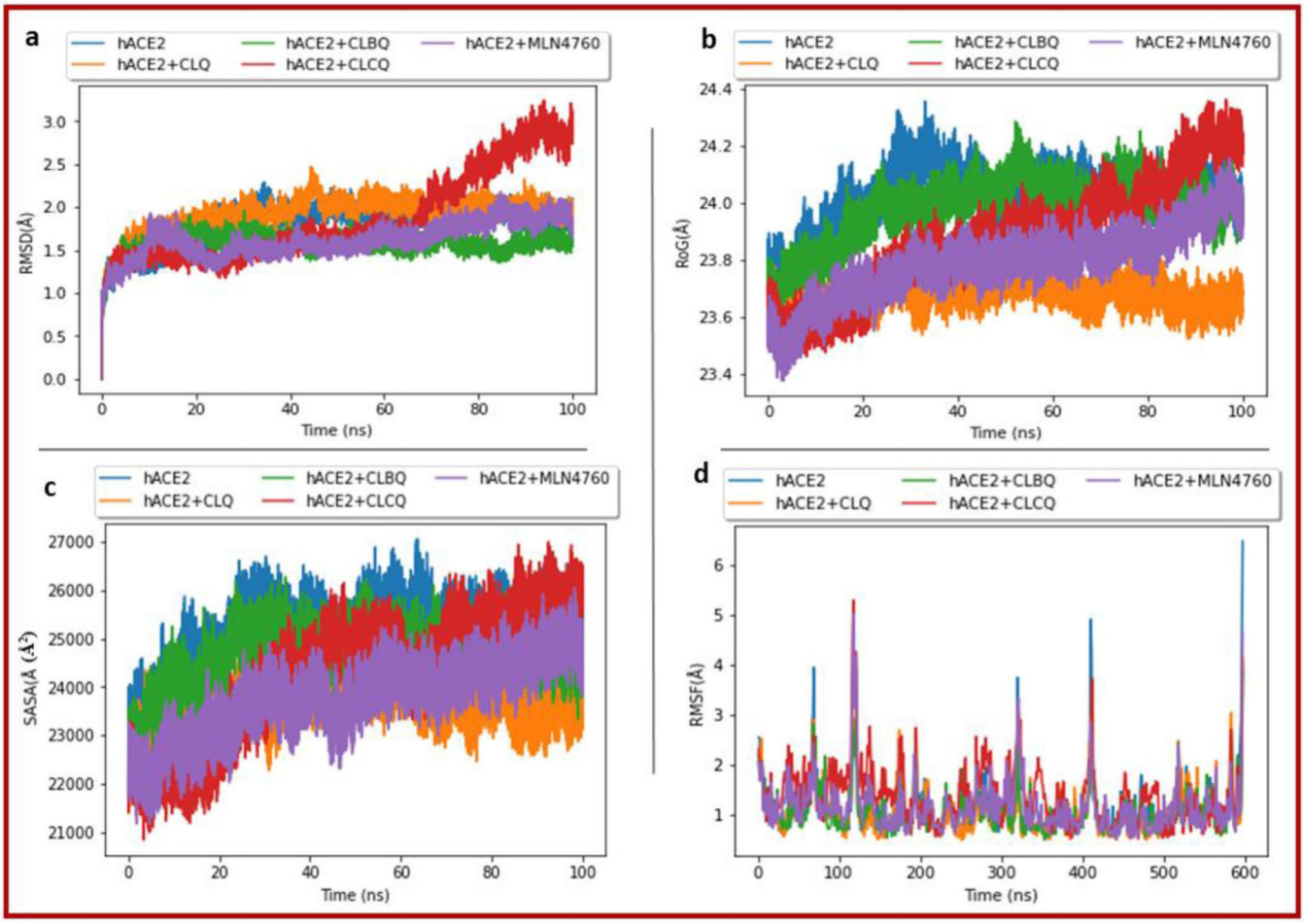

Figure 5.

Comparative a). RMSD b). RoG, c). SASA and d). RMSF profile plots of C-a atoms of the hACE2 with CLCQ, CLQ and CLBQ ligands-complexes calculated throughout 100 ns molecular dynamics simulation.

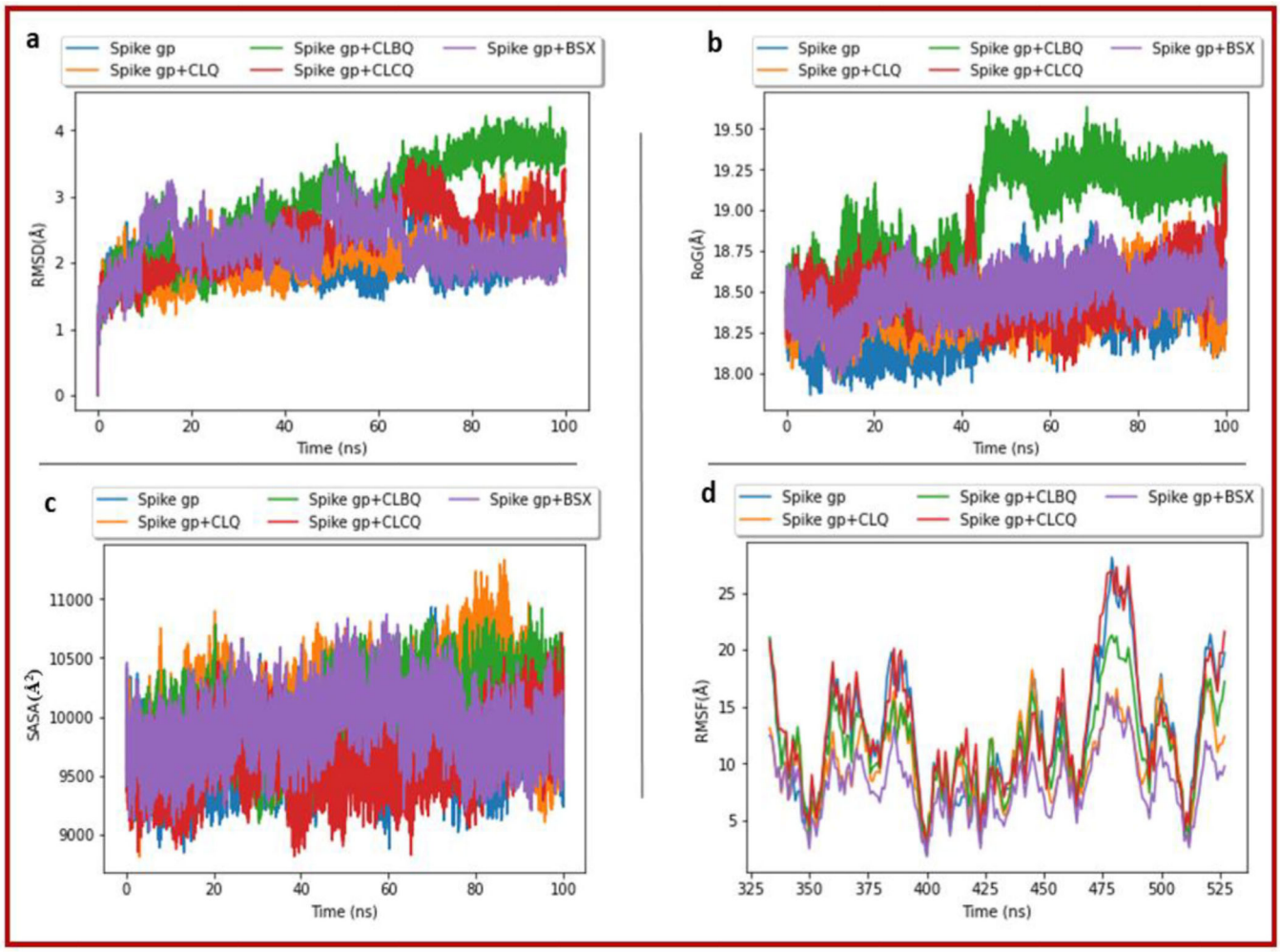

Figure 6.

Comparative a). RMSD b). RoG, c). SASA and d). RMSF profile plots of C-a atoms of the Spike gp with CLCQ, CLQ and CLBQ ligands-complexes calculated throughout 100 ns molecular dynamics simulation.

Table 1.

Thermodynamic Binding Free Energy Profiles for the ligands towards hACE2.

	Binding free energy (kcal/mol)			
	SARS-CoV-2 S_{gp}			
Energy components	**BSX**	**CLQ**	**CLBQ**	**CLCQ**
ΔE_{vdW}	−27.3 ± 2.3	−15.3 ± 4.9	−21.9 ± 4.6	−21.4 ± 1.7
ΔE_{elec}	−24.4 ± 4.3	−4.2 ± 0.3	−2.4 ± 0.4	−2.9 ± 0.4
ΔG_{gas}	−51.6 ± 5.1	−19.6 ± 0.5	−24.3 ± 4.4	−24.4 ± 3.4
ΔG_{solv}	25.7 ± 2.8	7.1 ± 2.8	7.5 ± 2.6	8.0 ± 2.0
ΔG_{bind}	−25.8 ± 2.9	−12.5 ± 4.7	−16.8 ± 4.0	−16.3 ± 1.8

Table 2.

Thermodynamic Binding Free Energy Profiles for the ligands towards SARS-CoV-2 Sgp.

	Binding free energy (kcal/mol)			
	hACE-2			
Energy components	**MLN-4760**	**CLQ**	**CLBQ**	**CLCQ**
ΔE_{vdW}	−41.7 ± 6.9	−35.7 ± 2.1	35.4 ± 1.7	−29.28 ± 1.8
ΔE_{elec}	54.6 ± 5.4	−16.0 ± 3.4	−6.0 ± 0.3	−3.38 ± 0.1
ΔG_{gas}	−77.9 ± 6.9	−46.8 ± 3.2	38.4 ± 2.1	−33.3 ± 3.1
ΔG_{solv}	85.6 ± 6.9	11.4 ± 2.4	8.0 ± 1.5	8.4 ± 2.3
ΔG_{bind}	−45.4 ± 5.8	−40.4 ± 2.8	34.4 ± 2.0	−24.8 ± 2.3

Table 3.

Calculated average values of parameter used to interpret structural stability for hACE-2 complexes.

	Average values			
Complex	**RMSD (Å)**	**RoG (Å)**	**SASA (Å^2)**	**RMSF (Å)**
hACE	1.81 ± 0.45	24.03 ± 2.34	25159.20 ± 100.02	1.14 ± 0.02
hACE2 + MLN	1.62 ± 0.32	23.79 ± 1.34	23783.34 ± 121.33	1.13 ± 0.73
hACE + CLQ	1.91 ± 0.03	23.69 ± 0.35	23670.52 ± 289.34	1.06 ± 0.01
hACE + CLBQ	1.57 ± 0.71	23.91 ± 3.01	24657.90 ± 202.34	1.05 ± 0.43
hACE+CLCQ	1.85 ± 0.04	23.90 ± 0.08	24657.54 ± 143.44	1.37 ± 0.24

Table 4.

Calculated average values of parameter used to interpret structural stability for SARS-CoV-2 S_{gp}. complexes.

	Average values			
Complex	**RMSD (Å)**	**RoG (Å)**	**SASA (Å^2)**	**RMSF (Å)**
Spike gp	2.06 ± 0.30	18.32 ± 2.44	9733.16 ± 78.56	12.49 ± 1.23
Spike gp + BSX	2.25 ± 0.45	18.48 ± 1.39	9908.32 ± 39.56	8.19 ± 0.35
Spike gp + CLQ	2.09 ± 0.54	18.41 ± 1.34	10065.65 ± 93.45	10.22 ± 0.44
Spike gp + CLBQ	2.86 ± 0.32	18.96 ± 0.98	10015.54 ± 103.34	11.46 ± 0.93
Spike gp + CLCQ	2.37 ± 0.11	18.48 ± 3.10	9657.32 ± 57.28	12.93 ± 1.02